Original paper

Sn-rich phosphates, kintoreite and plumbogummite, from the Ratibořské Hory Ag–Pb–Zn deposit, Czech Republic

Radana VRTIŠKOVÁ[1,2]*, Luboš VRTIŠKA[2], Jiří SEJKORA[2], Zdeněk DOLNÍČEK[2], Jakub TRUBAČ[3], Ladislav STRNAD[3]

[1] *Department of Geological Sciences, Faculty of Science, Masaryk University, Kotlářská 2, 611 37, Brno, Czech Republic; radana.vrtiskova@nm.cz*

[2] *Department of Mineralogy and Petrology, National Museum, Cirkusová 1740, 193 00 Prague 9, Czech Republic*

[3] *Institute of Geochemistry, Mineralogy and Mineral Resources, Faculty of Science, Charles University, Albertov 6, 128 43 Prague 2, Czech Republic*

* *Corresponding author*

Phosphates of the plumbogummite group (kintoreite and plumbogummite) with unusually high Sn contents have been discovered in a field in the area of reclaimed mine dumps at the abandoned Ag–Pb–Zn deposit Ratibořské Hory (South Bohemia Region, Czech Republic). These phosphates form very finely dispersed microscopic grains in the hydrothermal veins penetrating altered muscovite paragneisses in association with quartz, opal, pyromorphite, acanthite and more rarely galena, sphalerite, iodargyrite, imiterite, cuprite, mimetite, coronadite and unidentified Sn silicate. The studied Sn-rich phosphates can be divided into three groups: 1. Sn-rich kintoreite with the empirical formula (mean of the 14 point analyses) corresponds to $Pb_{1.05}(Fe_{2.51}Sn_{0.46}Zn_{0.06})_{\Sigma 3.03}(PO_4)_{1.55}(PO_3OH)_{0.45}(OH)_{6.00}$; 2. Sn-rich plumbogummite with empirical formula (mean of 6 analyses) $Pb_{1.14}(Al_{2.50}Sn_{0.52}Fe_{0.04})_{\Sigma 3.06}(PO_4)_{1.98}(PO_3OH)_{0.02}(OH)_{6.00}$; 3. (Sn,Al)-rich kintoreite with mean composition (calculated from 14 analyses) $(Pb_{0.95}Ca_{0.05})_{\Sigma 1.00}(Fe_{1.62}Sn_{0.90}Al_{0.62}Zn_{0.05})_{\Sigma 3.19}(PO_4)_{1.69}(SiO_4)_{0.21}(AsO_4)_{0.10}(OH)_{6.20}$. To date, no primary Sn minerals have been observed in the Ratibořské Hory ore deposit. Elevated Sn contents (up to 3040 ppm) in sphalerites from the Stará Vožice–Ratibořské Hory ore district, especially from the area with the occurrence of Sn-rich phosphates detected by La-ICP-MS during this research, probably indicate a primary source of Sn entering to the supergene processes.

Keywords: Sn-rich plumbogummite, Sn-rich kintoreite, Raman spectroscopy, Ag–Pb–Zn deposit, Ratibořské Hory, Czech Republic
Received: 10 June 2024; accepted: 3 December 2024; handling editor: R. Skála

1. Introduction

During our research of the abandoned ore deposit Ratibořské Hory (South Bohemia Region, Czech Republic), phosphates of the plumbogummite group with unusually high contents of Sn were discovered. The processes of weathering of Sn minerals and the mobility of Sn remain poorly understood, and, in general, supergene Sn minerals are very rare. The most common of these are varlamoffite-like minerals (e.g., Sharko 1971) and the hydroxides of the schoenfliesite subgroup. The conditions of the formation of minerals belonging to the schoenfliesite subgroup have been studied e.g., by Haase et al. (2021). This paper presents two previously proposed mechanisms for the formation of tin hydroxides. First, they may form as primary minerals in the late stages of high-temperature hydrothermal systems (Betterton et al. 1998) or in a magmatic stage (Åmli and Griffin 1972). Second, they occur as weathering products of primary tin minerals, especially sulphides (e.g., Betterton et al. 1998; Černý et al. 2001), but also tin borates (Nefedov et al. 1977; Aleksandrov 2010), tin alloys (Basciano et al. 1998), and potentially cassiterite (Nefedov et al. 1977). Rare unknown supergene Sn–Fe–As(–S)–O minerals are described by Moura et al. (2007) from granites of the Mangabeirra Massif in Brazil and by Kocourková-Víšková et al. (2014) from Kaňk near Kutná Hora in Czech Republic as the products probably formed by the alteration of a stannite group minerals. The stoichiometry of these phases does not correspond to the minerals of the alunite supergroup. To date, neither alunite supergroup minerals nor other secondary phosphates with high Sn contents have been observed.

Plumbogummite and kintoreite are members of the alunite supergroup with a general formula $AB_3(XO_4)_2(OH, H_2O)_6$. Position *A* is occupied by large mono- (Na^+, K^+, Rb^+, Ag^+, NH_4^+, H_3O^+, Tl^+), di- (Ca^{2+}, Sr^{2+}, Ba^{2+}, Pb^{2+}) or trivalent (Bi^{3+}, REE^{3+}) cations. The octahedrally coordinated position *B* is usually occupied by trivalent cations such as Fe^{3+}, Al^{3+}, Cr^{3+}, V^{3+} and Ga^{3+}, in some cases it may also contain di- (e.g., Cu^{2+} and Zn^{2+}), tetra- (Ge^{4+}) or pentavalent (Sb^{5+}) cations. At the tetrahedral *X*-sites are present mainly S^{6+}, P^{5+} and As^{5+}, even though minor contents of Si^{4+}, Cr^{6+} or Si^{4+} were also determined. In the

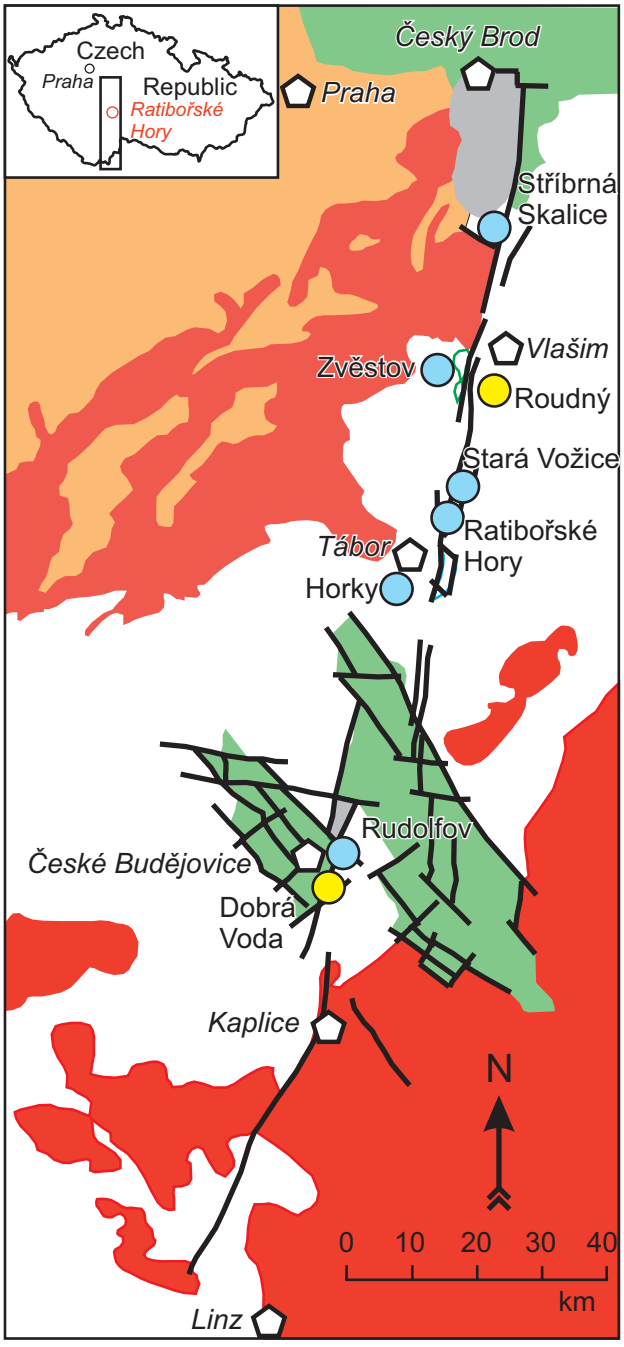

Upper Cretaceous sediments
Upper Carboniferous–Lower Permian
Central Bohemian Plutonic Complex
South Bohemian Plutonic Complex
Teplá–Barrandian Unit (Proterozoic–Paleozoic)
Moldanubian Unit (Proterozoic–Paleozoic)
Faults
Au-deposits
Ag-Pb-Zn deposits

case of significant contents of divalent cations in position *A* and a predominance of P or As in the tetrahedral position *X*, part of the anion groups are protonated to form $(PO_3OH)^{2-}$ or $(AsO_3OH)^{2-}$ groups. Part of the OH groups may be substituted by O^{2-}, F^- or H_2O (Jambor and Dutrizac 1983; Scott 1987; Pring et al. 1995; Rattray et al. 1996; Jambor 1999; Kolitsch and Pring 2001; Sejkora et al. 2001; Grey et al. 2008; Mills et al. 2008; Sato et al. 2008; Grey et al. 2009; Mills et al. 2009; Sejkora et al. 2009; Bayliss et al. 2010; Schlüter et al. 2014).

The contents of Sn in the minerals of the alunite supergroup have not yet been described and their study is the subject of our paper. This research builds on a previous study of Pb phosphates (pyromorphite and kintoreite) from the Ratibořské Hory ore deposit published by Vrtiška et al. (2019a).

2. Geological setting

Historical hydrothermal ore deposit Ratibořské Hory represented a southern part of the ore district Stará Vožice–Ratibořské Hory, with abandoned mines for silver ore, lying 8 km northeast of Tábor (South Bohemia Region, Czech Republic). Mining activity at this deposit seems to have begun already in the 13th or 14th century and ceased in the first half of the 19th century. Only maintenance work was carried out in the second half of the 19th century (Čech et al. 1952).

The Stará Vožice–Ratibořské Hory ore district is located within the Moldanubian unit of the Bohemian Massif, which represents an intensively metamorphosed crystalline complex with three stacked nappe units: Ostrong (Monotonous), Drosendorf (Variegated), and Gföhl (e.g. Fiala 1995; Franke 2000). The Ostrong and Drosendorf Units were metamorphosed under amphibolite-facies condition. The Ostrong Unit is dominated by paragneisses, whereas the Drosendorf Unit also contains bodies of marbles, orthogneisses, amphibolites, quartzites, and graphitic schists. The Gföhl Unit consists mainly of granulites with orthogneisses and minor eclogites and peridotites metamorphosed under granulite- to eclogite-facies conditions at about 340 Ma (e.g., Faryad et al. 2010; Friedl et al. 2011).

Hydrothermal ore veins of the Ratibořské Hory deposit are situated in the biotite paragneisses and migmatites of the Drosendorf Unit (western part), and muscovite-biotite paragneisses of the Ostrong Unit (eastern part). A prominent fault zone separates these two lithologies referred to as "Clay Cleft", which is part of a large brittle tectonic zone of the Blanice graben, an NNE–SSW trending, 200 km long tectonic zone (also called the Kouřim–Blan-

Fig. 1 Simplified geological map of the Blanice Graben and surrounding units with location of Au and Ag–Pb–Zn hydrothermal vein-type deposits (modified according to Zachariáš and Hübst 2012).

ice–Kaplice–Rödl fault zone) crossing all the Moldanubian units and extending from the Český Brod to Linz in Austria (Fig. 1). The faults of the Blanice graben have been repeatedly reactivated. The oldest identified tectonic activity is inferred to be Permo-Carboniferrous in age (Stephanian C to Autunian; Holub 2001), as has been suggested from the isolated islets of coal-bearing sediments. Therefore, the major tectonic movements in the Blanice graben must be of Permian age or younger (Zachariáš et al. 2009). Košler et al. (2001) studied a chilled microgranodiorite dike that cut Moldanubian paragneisses near of a major NNE–SSW fault of the Blanice graben. They suggest a minimum intrusive age of 270 ± 2 Ma ($^{40}Ar/^{39}Ar$ on hornblende), an origin from remelting of the lower crust and a temperature of less than 200 °C for the surrounding Moldanubian host rocks at the time of the microgranodiorite-dike intrusion. According to Brandmayr et al. (1995), the Blanice Graben is a part of a conjugated strike-slip ductile and fault system consisting of dextral (NW–SE) and sinistral (NE–SW) shear/fault zones originated under N–S oriented compression and E–W oriented extension. The Blanice Graben, in addition to the Stará Vožice–Ratibořské Hory ore district, hosts numerous other hydrothermal ore deposits (e.g., Au deposits Roudný and Dobrá Voda; Ag–Pb–Zn deposits Stříbrná Skalice, Rudolfov and many other minor occurrences.

The Ag–Pb–Zn ore district Stará Vožice–Ratibořské Hory is characterized by quartz–carbonate and rarely baryte gangue with abundant galena and sphalerite accompanied by Ag-rich minerals (including keno/argentotetrahedrite-(Fe), pyrargyrite, stephanite, argentite, native silver, rare pyrostilpnite and polybasite) and

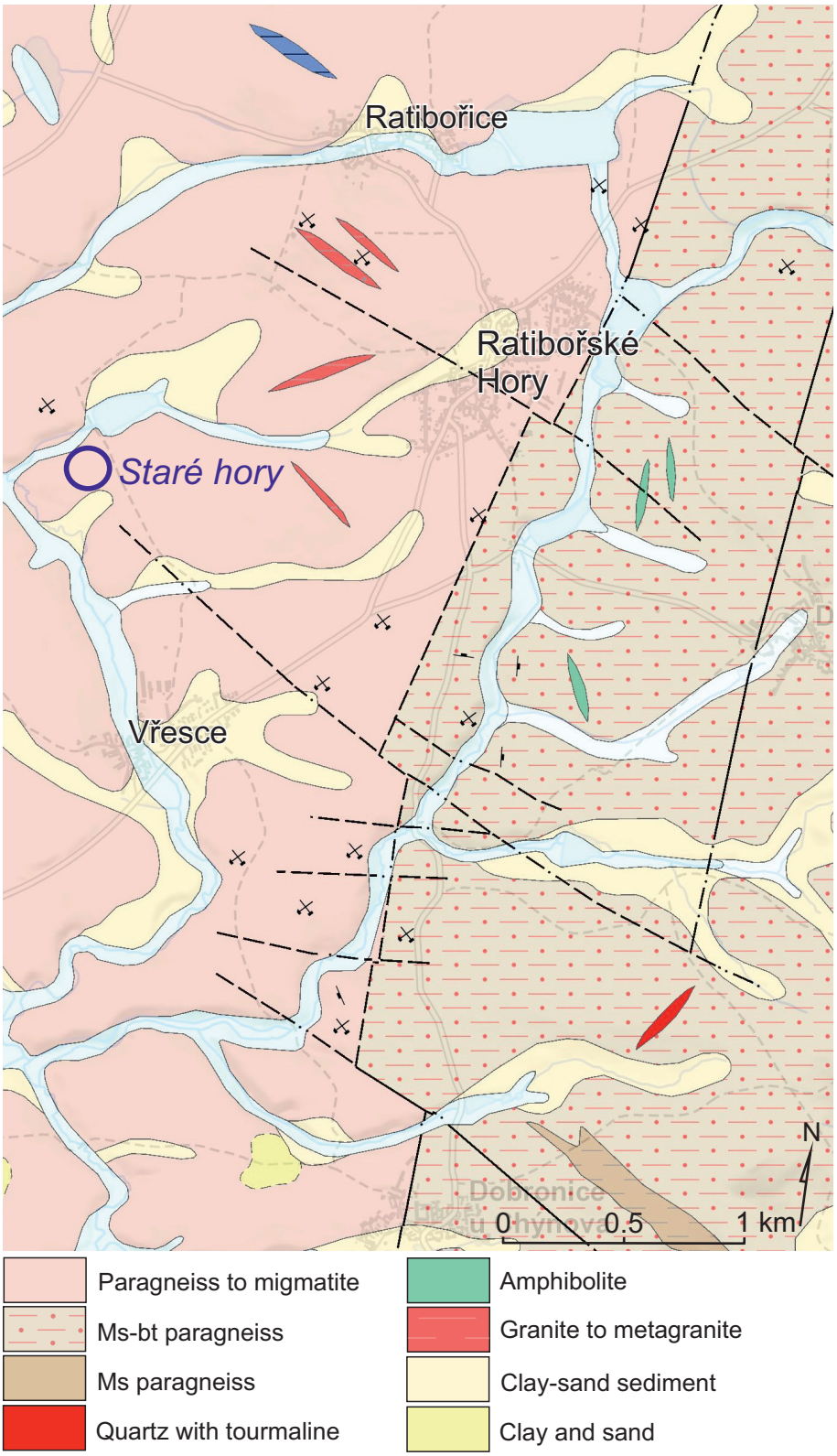

Fig. 2 Simplified geological map of the Ratibořské Hory deposit area showing the occurrence of phosphates in the Staré hory; adapted from the map server of the Czech Geological Survey; geological map 1 : 50 000; available at: https://mapy.geology.cz/geocr50/).

with minor Fe-sulphides (pyrite, chalcopyrite and arsenopyrite) (e.g., Čech et al. 1952; Šrein 1985; Velebil et al. 2016; Vrtiška et al. 2020). Occurrences of supergene minerals in this ore district were very rare; the described occurrences of anglesite, azurite, cerussite, erythrite, greenockite, hydrozincite, malachite, parasymplesite, and pyromorphite (e.g. Čech et al. 1952; Vrtiška et al. 2019b) were mostly formed by (sub)recent weathering of ore minerals in mine dumps. Recently, rich occurrences of supergene Pb minerals (pyromorphite, kintoreite-like minerals and cerussite) originating from supergene zone *in-situ* have been discovered at Staré hory near Ratibořské Hory (Vrtiška et al. 2019a).

3. Experimental

3.1. Occurrence and sample description

Samples with the phosphates of the plumbogummite group (kintoreite and plumbogummite) were collected in the field about 1.7 km WSW of Ratibořské Hory in a mining area called Staré hory (GPS: N 49°27.44', E 14°44.83'; Fig. 2). It is probably the oldest mining area in the Ratibořské Hory ore deposit, as evidenced by the NW–SE trending line of abundant remains of shallow shafts (Fig. 3a, b). The studied samples were collected during field research around former shaft dumps. The occurrence of pyromorphite and well crystallized kintoreite (without Sn contents) from this area was published by Vrtiška et al. (2019a). These samples were found about 50 m south from the occurrence of Sn-rich phosphates.

The studied phosphates form very finely dispersed microscopic grains in the hydrothermal veins penetrating altered muscovite paragneisses. These veins reach a thickness of up to 5 cm and are formed by crystals of white to colourless quartz up to 1 cm in size, milky to clear opal, *limonite*, and grey to black irregular grains of Ca-rich pyromorphite up to 5 mm in size (Fig. 4). Opal and quartz grains are coloured black in some parts by microscopic scaly aggregates of acanthite. Kintoreite and plumbogummite are dispersed mainly in the opal parts, which turn yellow to green-yellow in colour. In some samples, phosphates also penetrate the host rock (Fig. 5). Most of the studied phosphates are represented by almost pure kintoreite, which forms orange-yellow and yellow radial aggregates up to 100 μm. Its chemical composition is almost identical to that found in this area by Vrtiška et al. (2019a) for the well-crystallised varieties of kintoreite.

Only a minor part of the studied phosphates from the plumbogummite group have increased Sn contents and are further divided according to chemical composition into three groups (Fig. 6). More rarely, grains of galena, sphalerite, iodargyrite, imiterite, cuprite, mimetite and zoned aggregates of coronadite have been observed in the association. Exceptionally, irregular aggregates and veins of unidentified heterogenous Sn silicate up to 300

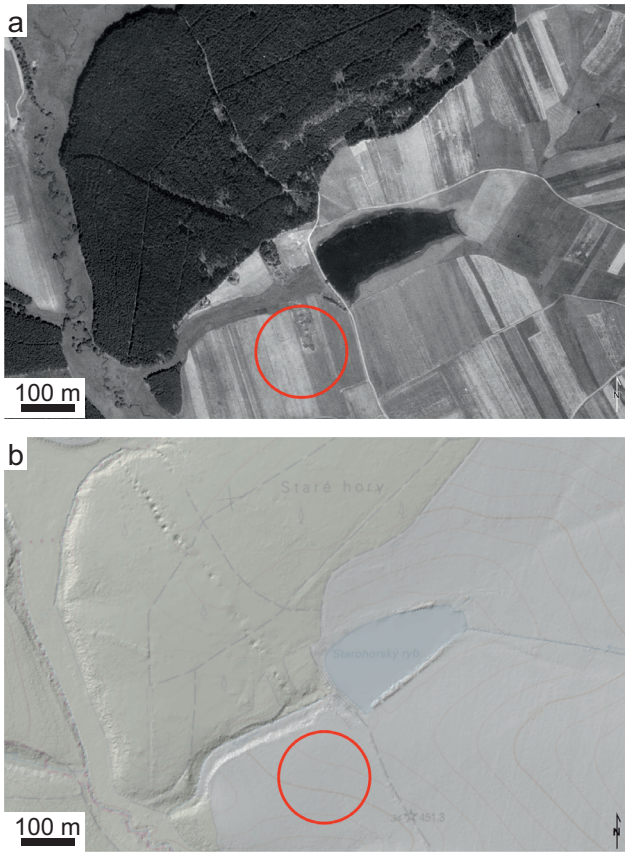

Fig. 3a – The area of Staré hory as depicted in the aerial photograph showing the visible (now plated) remains of mining; year 1953 (available at https://geoportal.gov.cz). **b** – Digital relief model of the 5th generation of the same area with a visible line of historical mining works and marked place with the occurrence of the studied minerals. The model was made between 2009–2013 (available at https://ags.cuzk.cz/geoprohlizec).

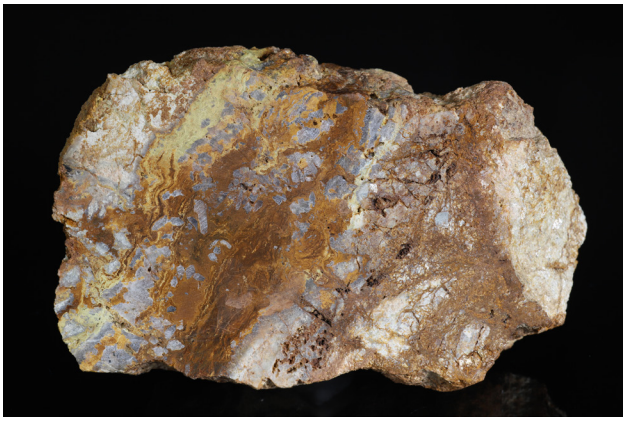

Fig. 4 Hydrothermal vein with phosphates in an altered paragneiss. The vein consists of white to colourless quartz, opal with *limonite*, grey to black irregular grains of Ca-rich pyromorphite and yellow powdery aggregates of Sn-rich phosphates; sample size 110 × 65 mm. Photo: L. Vrtiška.

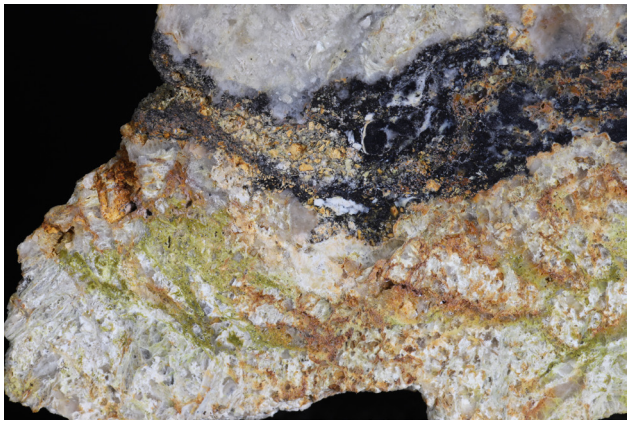

Fig. 5 Detail of hydrothermal vein formed by quartz and colourless to white opal. Opal is locally black coloured by abundant inclusions of acanthite. The Sn-rich phosphates are dispersed mainly in the opal parts and host rock, which turn yellow to green-yellow in colour; image width 60 mm. Photo: L. Vrtiška.

μm in size were observed (Fig. 7). Its chemical composition is a combination of SnO_2 (58.98–66.09 wt. %), SiO_2 (18.78–26.74 wt. %) and minor CaO (0.87–1.07 wt. %).

The Sn-rich kintoreite is the most common mineral with Sn content in the studied material from the Ratibořské Hory. It occurs in opal or in host rocks forming yellow to green-yellow finely dispersed irregular spherical grains, usually up to 10 μm in size, which often form irregular oblong clusters up to 300 μm (Fig. 8a, b). These aggregates are zoned in some places in the BSE image, with darker edges containing less Sn. The Sn-rich kintoreite aggregates in association with pure kintoreite

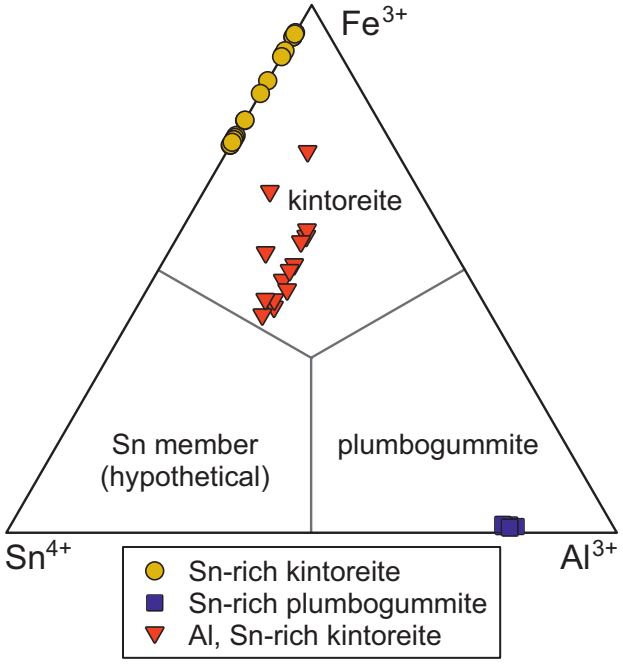

Fig. 6 Ternary diagram of Fe, Al, and Sn contents (*apfu*) in the studied phosphates from the plumbogummite group from Ratibořské Hory.

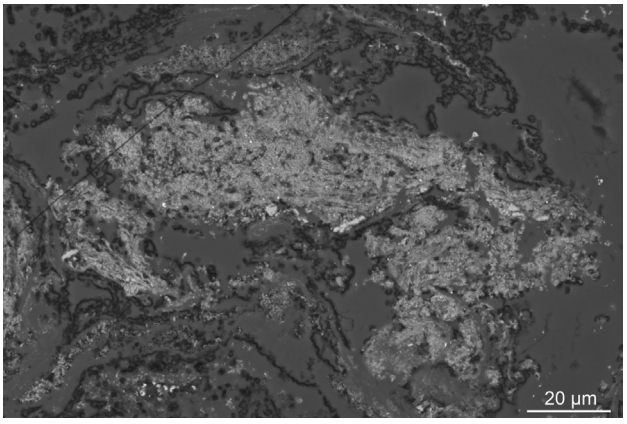

Fig. 7 Irregular aggregates of an unidentified heterogenous Sn-silicate (light grey) in opal (dark grey); BSE photo: L. Váchová.

and opal in places form a concentric "*agate-like*" texture. Besides Fe end-member compositions (Sn-rich kintoreite), the Al-rich grains (Sn,Al-rich kintoreite) were also found in the studied material.

Much rarer Sn-rich plumbogummite forms solitary blue-grey spherical grains up to 5 μm or their clusters

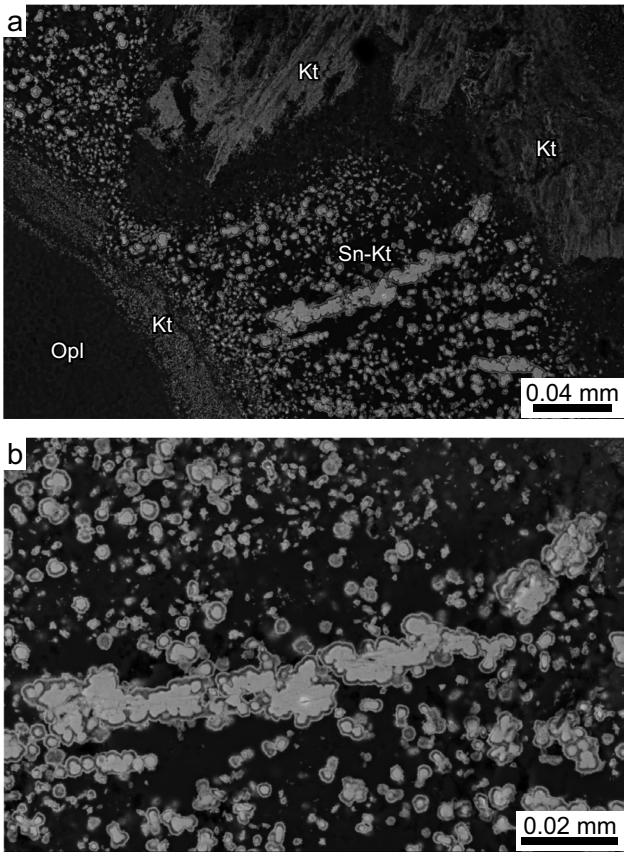

Fig. 8a – Spherical aggregates and their clusters of Sn-rich kintoreite (Sn-Kt) in the diagonal part of the photo, surrounded by more finely dispersed "pure" kintoreite (Kt); **b** – Sn-rich kintoreite aggregates may be zoned in places, darker rims contain less Sn; BSE photo: L. Váchová.

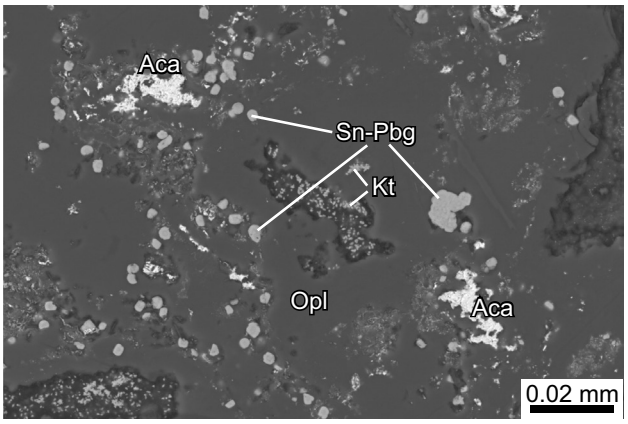

Fig. 9 Sn-rich plumbogummite (Sn-Pbg) in association with acanthite (Aca), "pure" kintoreite (Kt) and opal (Opl); BSE photo: L. Váchová.

up to 25 μm in size in opal in association with acanthite (Fig. 9).

3.2. Methods

Backscattered electron photos (BSE) were taken in the low-vacuum mode of the Hitachi S-3700N scanning electron microscope under the following conditions: accelerating voltage 17 kV and emission current 5800 nA (National Museum, Prague).

The chemical composition of studied minerals was determined on polished and carbon-coated fragments mounted in an epoxy cylinder using a Cameca SX 100 electron microprobe (National Museum, Prague). The instrument was operated in wavelength-dispersive mode at an accelerating voltage of 15 kV, beam current of 15 nA, and beam diameter of 2 μm. The following X-ray lines and standards were selected: *K*α lines: P, Ca (apatite), Si, Al (sanidine), Fe (hematite), Zn (ZnO); *M*α lines: Pb (vanadinite); *L*α lines: As (clinoclase), Sn (Sn). Other elements (Mg, Na, K, Y, Cl, Mn, Bi, In, S, Sr, U, V, Cu, Co, Ba, Th, F, Cr, N, Ni) were sought but not detected. Counting times were 10–20 s on peak and half of this time for each background position. The raw intensities were converted to the concentrations automatically using *PAP* (Pouchou and Pichoir 1985) matrix-correction algorithm. Water could not be analysed directly because of the very small amount of material available; the H_2O contents were calculated by the stoichiometry of ideal formulae and charge balance. Lower totals after adding the calculated water contents and a wide range of analytical totals of studied samples reflect (i) partial dehydration of samples in vacuum of EPMA chamber and (ii) uneven surface of samples.

Trace elements (Sn, Ga, Ge) in the galena were determined by means of ICP-MS analysis. The sample was digested in 10 ml HF (49 % v/v) and 3 ml HNO_3 (70 % v/v) in PTFE vessels (Savillex, Minnetonka, USA) overnight on a hot plate (150 °C). After the vessel was opened, the sample was evaporated to approx. 0.5 ml of the digest, which was dissolved in 2 % v/v HNO_3 and transferred to a 50 ml volumetric flask. All the samples (and procedural blanks) were further diluted five-fold by 2 % v/v HNO_3. All the acids used in the dissolution procedure were reagent grade (Merck, Germany and Penta Chrudim, Czech Republic) and double distilled. Purified water obtained from a Millipore system (Millipore, USA) was used for all the dilutions. All the solutions were stored in HDPE (Nalgene) bottles. A standard configuration of ICP-MS iCap Thermo Fisher equipped with a water-cooled (~ 5 °C) spray chamber with Meinhard-type nebuliser was utilised to analyse the solutions (modified after Strnad et al. 2005).

In-situ Sn, Ga, Ge analyses of sphalerite were performed on a quadrupole ICP-MS iCAP-Q (Thermo Bremen, Germany) coupled to a CETAC LSX-213 nm laser microprobe installed at the Charles University in Prague. The Al-3 sulfide reference material (provided by Mr. D. Savard, Univ. Quebec Chicoutimi, LabMaTer, Canada) was used as a calibrator and all analyses (spot of diameter 50 μm) were normalized to ^{33}S signal as internal standard. The sample introduction system and analytical protocol followed similar procedures described by Strnad et al. (2009, 2012).

Raman spectra of the studied sample were collected at room temperature in the range 50–4000 cm^{-1} using a DXR dispersive Raman Spectrometer (Thermo Scientific) mounted on a confocal Olympus microscope (National Museum, Prague). The Raman signal was excited by an unpolarized 532 nm diode-pumped solid-state laser and detected by a CCD detector. The experimental parameters were: 50× objective (estimated diameter of the laser spot less than 0.7 μm), 10 s exposure time, 1000 exposures, 400 lines/mm grating (spectral resolution 8.1–18.7 cm^{-1}), 25 μm pinhole spectrograph aperture and 7 mW laser power level. The data were repeatedly acquired from different grains in order to obtain a representative spectrum with the best signal-to-noise ratio. Eventual thermal damage of the measured point was excluded by visual inspection of the excited surface after measurement, by observation of possible decay of spectral features at the start of excitation and by checking for thermal downshift of Raman lines. The instrument was set up using a software-controlled calibration procedure using multiple neon emission lines (wavelength calibration), multiple polystyrene Raman bands (laser frequency calibration), and standardized white-light sources (intensity calibration).

4. Results and discussion

4.1. Chemical composition

Chemical composition of all studied Sn-containing samples agrees well with the ideal formula of alunite

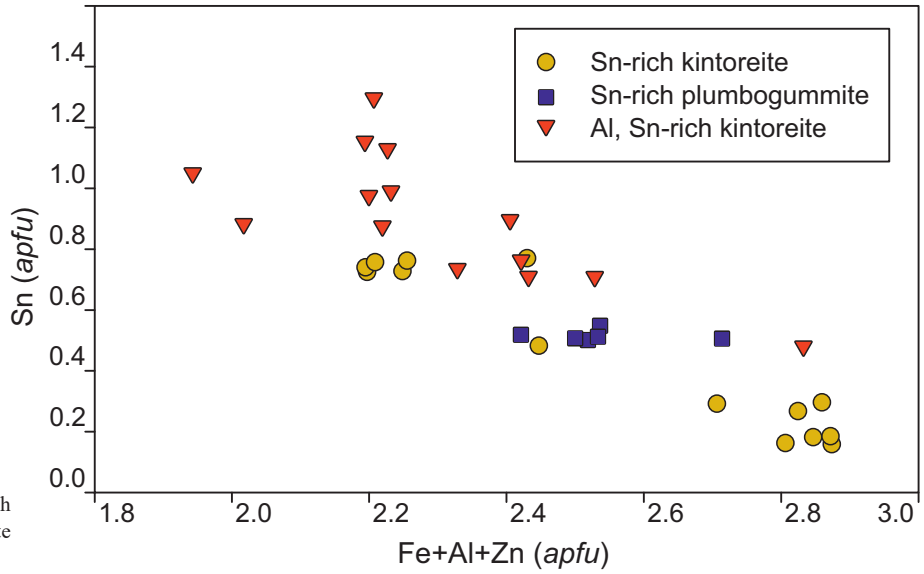

Fig. 10 The (Fe+Al+Zn) vs. Sn graph (*apfu*) for kintoreite and plumbogummite from Ratibořské Hory.

supergroup minerals $AB_3(XO_4)_2(OH, H_2O)_6$. The Sn contents correlate well with Fe+Al+Zn ones, which implies that Sn occupies *B*-position (Fig. 10). As same as in the case of Ge^{4+} contents in galloplumbogummite (Schlüter et al. 2014), we assume that Sn^{4+} components on the trivalent cation site of studied samples are compensated by a change of ratio of $(PO_3OH)^{2-}/(PO_4)^{3-}$ groups in crystal structure. An additional excess of positive charge is probably compensated by the increased amount of OH groups.

Table 1 provides the chemical composition of Sn-rich kintoreite from Ratibořské Hory. In the *A*-site it contains only Pb (1.01–1.13 *apfu*), *B*-site is dominated by Fe (2.10–2.85 *apfu*) with contents of Sn (0.16–0.77 *apfu*; up to 15.13 wt. % SnO_2; Fig. 7) and Zn (up to 0.11 *apfu*). The empirical formula (based on P = 2 *apfu*; mean of the 14 point analyses) corresponds to $Pb_{1.05}(Fe_{2.51}Sn_{0.46}Zn_{0.06})_{\Sigma 3.03}(PO_4)_{1.55}(PO_3OH)_{0.45}(OH)_{6.00}$.

In Sn-rich plumbogummite (Tab. 2) the *A*-site contains only Pb (1.06–1.22 *apfu*). The *B*-site is occupied by Al (2.37–2.68 *apfu*), Sn (0.51–0.55 *apfu*; up to 11.27 wt. % SnO_2) and Fe (up to 0.05 *apfu*). Its empirical formula (mean of 6 analyses) can be expressed on the basis of P = 2 *apfu* as $Pb_{1.14}(Al_{2.50}Sn_{0.52}Fe_{0.04})_{\Sigma 3.06}(PO_4)_{1.98}(PO_3OH)_{0.02}(OH)_{6.00}$.

The chemical composition of Sn,Al-rich kintoreite is distinctly more complex (Tab. 3), the *A*-site is occupied by Pb (0.84–1.06 *apfu*) and Ca (up to 0.07 *apfu*), *B*-site is dominated by Fe (1.30–2.35 *apfu*) with high Al (0.33–0.74 *apfu*), Sn (0.47–1.29 *apfu*; up to 24.92 wt. % SnO_2), and low Zn (up to 0.09 *apfu*). The *X*-site is dominated by P (1.52–1.91 *apfu*) with minor contents of Si (0.06–0.32 *apfu*) and As (up to 0.24 *apfu*). Its mean composition (calculated from 14 analyses on the base of P+Si+As=2 *apfu*) is $(Pb_{0.95}Ca_{0.05})_{\Sigma 1.00}(Fe_{1.62}Sn_{0.90}Al_{0.62}Zn_{0.05})_{\Sigma 3.19}(PO_4)_{1.69}(SiO_4)_{0.21}(AsO_4)_{0.10}(OH)_{6.20}$.

Tab. 1 Chemical composition of Sn-rich kintoreite (wt. %)

	mean	1	2	3	4	5	6	7	8	9	10	11	12	13	14
PbO	31.70	32.66	31.89	32.77	33.40	31.63	33.22	33.10	31.90	31.14	30.76	30.50	29.82	29.91	31.05
ZnO	0.61	0.22	0.32	0.29	0.40	0.24	0.36	0.27	0.65	0.90	0.88	0.99	1.21	0.97	0.90
Fe_2O_3	27.17	31.76	31.35	31.82	31.32	30.62	30.84	30.97	26.44	22.45	22.85	22.09	22.07	22.77	22.97
SnO_2	9.33	3.33	3.46	3.87	3.85	5.51	6.34	6.10	10.07	14.53	14.48	14.68	15.04	15.13	14.26
P_2O_5	19.26	19.78	20.06	20.05	19.63	19.42	20.49	19.42	19.67	18.88	18.75	18.68	18.72	18.70	17.45
H_2O*	7.89	8.36	8.83	8.50	8.12	7.90	8.69	7.51	8.39	7.78	7.54	7.67	7.64	7.41	7.24
total	95.96	96.11	95.91	97.30	96.72	95.32	99.94	97.37	97.12	95.68	95.26	94.61	94.50	94.89	93.87
Pb	1.046	1.050	1.011	1.039	1.082	1.036	1.031	1.084	1.031	1.049	1.043	1.038	1.013	1.017	1.132
Zn	0.056	0.019	0.028	0.025	0.036	0.022	0.031	0.024	0.058	0.083	0.082	0.092	0.113	0.090	0.090
Fe	2.507	2.854	2.778	2.821	2.836	2.803	2.676	2.835	2.390	2.114	2.166	2.102	2.096	2.165	2.340
Sn	0.456	0.159	0.162	0.182	0.185	0.267	0.291	0.296	0.482	0.725	0.727	0.740	0.757	0.762	0.770
Σ *B*-site	3.019	3.032	2.969	3.028	3.057	3.092	2.998	3.155	2.929	2.922	2.976	2.935	2.965	3.017	3.200
PO_4	1.550	1.337	1.062	1.321	1.483	1.593	1.316	1.905	1.276	1.506	1.660	1.530	1.566	1.758	2.000
PO_3OH	0.450	0.663	0.938	0.679	0.517	0.407	0.684	0.095	0.724	0.494	0.340	0.470	0.434	0.242	0.000
OH	6.000	6.000	6.000	6.000	6.000	6.000	6.000	6.000	6.000	6.000	6.000	6.000	6.000	6.000	6.543

H_2O* – contents calculated by valence balance and stoichiometry from the ideal formula; calculated empirical formulae are based on P = 2 *apfu*.

Tab. 2 Chemical composition of Sn-rich plumbogummite (wt. %)

	mean	1	2	3	4	5	6
PbO	34.73	35.06	36.38	35.44	33.77	33.70	34.04
Fe_2O_3	0.41	0.38	0.48	0.40	0.52	0.28	0.38
Al_2O_3	17.45	17.02	16.88	18.40	16.92	17.16	18.31
SnO_2	10.81	11.19	10.27	10.45	11.10	10.55	11.27
P_2O_5	19.44	18.95	19.00	19.14	19.84	19.31	20.39
H_2O*	7.43	7.44	7.27	7.96	8.14	7.62	8.01
total	90.26	90.04	90.28	91.79	90.29	88.62	92.40
Pb	1.136	1.177	1.218	1.178	1.083	1.110	1.062
Fe	0.037	0.036	0.045	0.037	0.047	0.026	0.033
Al	2.499	2.501	2.474	2.677	2.375	2.474	2.500
Sn	0.524	0.556	0.509	0.514	0.527	0.515	0.521
Σ *B*-site	3.060	3.093	3.028	3.228	2.948	3.015	3.054
PO_4	1.976	2.000	2.000	2.000	1.536	1.779	1.806
PO_3OH	0.024	0.000	0.000	0.000	0.464	0.221	0.194
OH	6.000	6.187	6.028	6.554	6.000	6.000	6.000

H_2O* – contents calculated by valence balance and stoichometry from the ideal formula; calculated empirical formulae are based on P = 2 *apfu.*

4.2. Raman spectroscopy

The experimental Raman spectra of all types of kintoreite (*"pure"*, Sn- and Sn,Al-rich) from the Ratibořské Hory are close to each other (Fig. 11, Tab. 4); this confirms that the studied Sn-containing phosphates exhibit also kintoreite-type of the crystal structure. Small differences in the relative intensity of individual bands are probably caused by the different orientations of studied grains. The following interpretation of of Raman bands is based on the papers of Farmer (1974), Pechkovski et al. (1981), Nakamoto (2009), Frost et al. (2010, 2013) and Vrtiška et al. (2022). Samples in the following text are labelled as KI (*"pure"* kintoreite without Sn), SN (Sn-rich kintoreite) and SA (Sn,Al-rich kintoreite). A broad Raman band at 3230 (KI) with a shoulder at 2936 (3226, 2942 SN, and 3220, 3047 SA) cm^{-1} are assigned to the ν OH stretching vibrations of OH groups. Bands at 1129 and 1074 (1077 SN, 1132 and 1077 SA) cm^{-1} are attributed to the ν_3 $(PO_4)^{3-}$ triply degenerated antisymmetric stretching vibrations, and that at 1006 cm^{-1} (identical wavenumber for all samples) to the ν_1 $(PO_4)^{3-}$ symmetric stretching vibrations. The ν_4 (δ) $(PO_4)^{3-}$ bending vibrations relate to the bands at 643, 576 and 553 (611, 578, 555 SN and 614, 577, 555 SA) cm^{-1}, and the ν_2 (δ) $(PO_4)^{3-}$ bending vibrations with the bands at 446 and 426 (443, 428 SN and 445, 427 SA) cm^{-1}. The possible presence of $(PO_3OH)^{2-}$ groups in kintoreite may cause the shift of the bands to higher wavenumbers than in the case of isolated PO_4 groups (Nakamoto 2009; Frost et al. 2010). Otherwise, it is not easy to distinguish between the vibration modes of the $(PO_4)^{3-}$ and $(PO_3OH)^{2-}$ groups. According to Pechkovski

Tab. 3 Chemical composition of Sn,Al-rich kintoreite (wt. %)

	mean	1	2	3	4	5	6	7	8	9	10	11	12	13	14
CaO	0.40	0.27	0.41	0.36	0.37	0.37	0.34	0.41	0.36	0.50	0.41	0.54	0.40	0.43	0.41
PbO	28.98	30.85	30.27	30.37	30.57	28.33	29.13	29.25	29.72	27.79	27.68	27.97	28.57	28.08	27.14
ZnO	0.59	0.57	0.51	0.57	0.48	0.99	0.78	0.61	0.59	0.48	0.47	0.56	0.60	0.49	0.53
Fe_2O_3	17.76	24.44	19.57	18.91	18.13	21.96	16.97	16.66	17.51	18.12	15.92	15.39	15.42	15.02	14.58
Al_2O_3	4.32	2.85	4.46	4.51	4.33	2.34	4.69	4.74	4.78	3.47	5.07	4.50	4.86	5.03	4.79
SnO_2	18.50	9.28	14.17	14.46	14.98	15.67	18.51	20.22	17.84	19.96	20.22	23.28	22.46	23.05	24.92
SiO_2	1.72	0.47	1.44	1.04	1.35	1.16	1.53	2.15	1.61	1.76	2.18	2.51	1.93	2.43	2.47
As_2O_5	1.53	0.48	0.00	1.27	0.38	2.73	2.71	4.23	0.05	3.14	1.52	3.35	1.08	0.46	0.00
P_2O_5	16.49	17.64	17.32	17.38	17.55	16.47	16.61	16.60	16.97	15.40	15.86	16.00	15.91	15.79	15.29
H_2O	7.65	7.59	7.61	7.40	7.63	7.44	7.89	9.56	7.93	7.60	7.68	8.69	8.26	8.20	8.57
total	97.92	94.44	95.76	96.27	95.77	97.46	99.16	104.43	97.36	98.22	97.01	102.79	99.49	98.98	98.70
Ca	0.052	0.037	0.055	0.047	0.048	0.048	0.043	0.048	0.048	0.065	0.054	0.065	0.054	0.057	0.057
Pb	0.947	1.061	1.012	0.996	1.003	0.923	0.922	0.855	1.000	0.910	0.909	0.846	0.964	0.943	0.948
Σ *A*-site	0.999	1.098	1.067	1.043	1.052	0.971	0.965	0.903	1.048	0.975	0.962	0.911	1.017	1.000	1.005
Zn	0.053	0.054	0.047	0.051	0.043	0.088	0.068	0.049	0.054	0.043	0.042	0.046	0.056	0.045	0.051
Fe	1.622	2.350	1.829	1.733	1.663	1.999	1.502	1.362	1.647	1.659	1.461	1.301	1.454	1.409	1.424
Al	0.618	0.429	0.653	0.648	0.622	0.334	0.650	0.607	0.704	0.498	0.729	0.596	0.718	0.739	0.732
Sn	0.896	0.473	0.702	0.702	0.728	0.756	0.868	0.876	0.889	0.968	0.983	1.043	1.122	1.146	1.289
Σ *B*-site	3.188	3.305	3.230	3.135	3.057	3.177	3.087	2.893	3.294	3.168	3.215	2.985	3.349	3.340	3.496
SiO_4	0.208	0.060	0.179	0.127	0.165	0.140	0.180	0.234	0.201	0.214	0.266	0.282	0.242	0.303	0.320
AsO_4	0.097	0.032	0.000	0.081	0.024	0.173	0.167	0.240	0.003	0.200	0.097	0.197	0.071	0.030	0.000
PO_4	1.695	1.908	1.821	1.792	1.604	1.687	1.465	0.604	1.796	1.586	1.637	1.013	1.687	1.667	1.680
PO_3OH	0.000	0.000	0.000	0.000	0.207	0.000	0.189	0.922	0.000	0.000	0.000	0.508	0.000	0.000	0.000
Σ *T*-site	2.000	2.000	2.000	2.000	2.000	2.000	2.000	2.000	2.000	2.000	2.000	2.000	2.000	2.000	2.000
OH	6.198	6.471	6.301	6.014	6.000	6.001	6.000	6.000	6.613	6.165	6.244	6.000	6.906	6.818	7.416

H_2O* – contents calculated by valence balance and stoichiometry from the ideal formula; calculated empirical formulae are based on the sum of (Si + As + P) = 2 *apfu.*

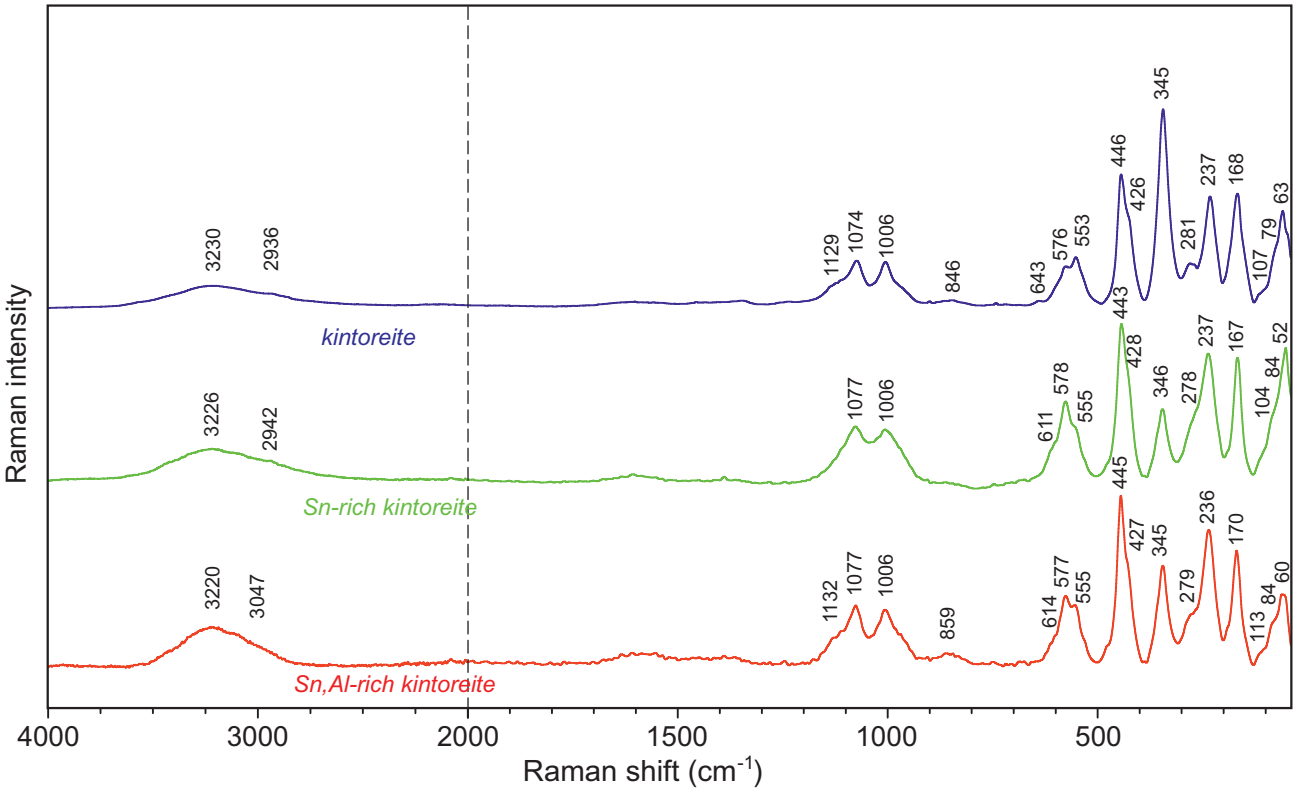

Fig. 11 Raman spectra of kintoreite samples from Ratibořské Hory (split at 2000 cm^{-1}), the spectra are vertically shifted for clarity.

et al. (1981), the bands for each of these groups occur in the close positions or form part of a broader band profile. An intensive band at 345 (346 SN and 345 SA) cm^{-1} may be related to the metal (Pb,Fe,Al)-oxygen stretching vibrations; those at 281, 237 (278, 237 SN and 279, 236 SA) cm^{-1} are attributed to metal-oxygen bending vibrations with possible overlap with vibrations of the hydrogen bonds formed between the hydroxyl units and the phosphate units. The bands observed below 200 cm^{-1} (168, 107, 79, 83 KI, 137, 104, 84, 52 SN and 170, 113, 84, 60 SA) may be described as lattice modes. Raman spectra of Sn-rich plumbogummite were measured but were not suitable for publication due to high fluorescence.

Tab. 4 Tentative assignment of Raman spectra of kintoreite from Ratibořské Hory

kintoreite*	Sn-rich kintoreite*	Sn,Al-rich kintoreite*	tentative assignment
3230	3226	3220	ν OH stretching vibrations
2936	2942	3047	
1129		1132	ν_3 $(PO_4)^{3-}$ stretching vibrations
1074	1077	1077	
1006	1006	1006	ν_1 $(PO_4)^{3-}$ stretching vibration
846		859	libration modes
643	611	614	ν_4 (δ) $(PO_4)^{3-}$ bending vibrations
576	578	577	
553	555	555	
446	443	445	ν_2 (δ) $(PO_4)^{3-}$ bending vibrations
426	428	427	
345	346	345	Pb–O and Fe–O stretching vibrations
281	278	279	Pb–O and Fe–O bending vibrations and/or vibrations of hydrogen bonds P–OH
237	237	236	
168	167	170	lattice modes
107	104	113	
79	84	84	
63	52	60	

*Band positions in cm^{-1}

Tab. 5 Contents of selected trace elements (in ppm) in sphalerites from the Stará Vožice (SV) – Ratibořské Hory (RH) ore district (N = 6)

Locality	Colour	Sn mean	Sn range	Ga mean	Ga range	Ge mean	Ge range
RH – Matyáš Mine	yellow	1.43	0.28–3.45	1.88	0.11–3.89	2.16	0.16–10.3
RH	red–yellow	1.37	0.00–7.09	0.24	0.00–0.88	1.13	0.01–4.00
SV – Marie Mine	brown	16.3	0.72–87.7	25.3	10.7–43.2	9.42	3.07–18.6
SV	brownish black	6.34	0.32–35.9	8.19	5.64–17.6	0.66	0.24–2.46
SV	black	11.9	2.04–56.1	11.2	8.15–13.8	1.43	0.54–2.02
RH	black	421	173–955	93.6	20.0–168	69.7	4.18–139
RH – Staré hory	black	1110	1.92–3040	9.19	3.89–15.0	17.1	1.73–64.1

4.3. Sources of Sn and the formation of the association

Tin occurs in nature mainly in primary minerals, mostly in cassiterite, but also in others, namely in sulphides (kësterite, stannite, franckeite, cylindrite, etc.). However, in general, supergene tin minerals are very rare. Moreover, no primary Sn minerals have been observed in the Ratibořské Hory ore deposit. The increased Sn contents in galena and especially in sphalerite are mentioned by Pačes (1958) based on the qualitative spectrographic analysis from the Stará Vožice (northern part of the Stará Vožice–Ratibořské Hory ore district). Following this information, were measured the Sn contents (and other trace elements) using LA-ICP-MS in one sample of galena and in 7 samples of different types of sphalerite from the material obtained in the area of occurrence of Sn-rich phosphates in Staré hory and from other parts of the Stará Vožice–Ratibořské Hory ore district. Only very low Sn concentrations (under 1 ppm) were detected in galena from the Staré hory area. In the studied sphalerites, the highest Sn contents (up to 3040 ppm) were measured in black-coloured sphalerite samples found in the area of Sn-rich phosphate occurrence in the Staré hory (Tab. 5). Elevated Sn contents (up to 955 ppm) were also observed in samples of black sphalerite from the Ratibořské Hory. Dark brown to black sphalerites from the neighbouring Stará Vožice ore district show significantly lower Sn contents (up to 88 ppm). The lowest Sn contents were found in yellow and yellow-orange sphalerites from Ratibořské Hory (up to 7 ppm).

The detected Sn contents in sphalerites from the Stará Vožice–Ratibořské Hory ore district, especially from the area with the occurrence of Sn-rich phosphates, probably indicate a primary source of Sn entering to the supergene processes. The abundant opal and locally present heterogeneous Sn-silicates indicate the possibility of formation of the studied Sn-containing phosphates from Si-rich gels, similarly, as described by Majzlan et al. (2012) in the case of the crystallization of supergene bukovskýite in the Kutná Hora ore district.

The high Sn contents in studied sphalerites are also accompanied by increased contents of Ga and Ge (Tab. 5). These elements may enter the crystal structure of plumbogummite group minerals, specifically the galloplumbogummite (Schlüter et al. 2014). However, in the studied Sn-rich phosphates, these elements were not detected by EPMA and due to their minimum size the use of LA-ICP-MS is not possible.

5. Conclusions

Studied minerals of the plumbogummite group (plumbogummite and kintoreite), discovered in a field in the area of reclaimed mine dumps at the abandoned Ag–Pb–Zn deposit Ratibořské Hory (Czech Republic), contain unusually high Sn contents (up to 1.29 *apfu* or 24.92 wt. % SnO_2 respectively). To date, neither alunite supergroup minerals nor other secondary phosphates with high Sn contents have been observed. Sn, on the basis of good correlation with Fe+Zn+Al, occupies the *B*-position of the studied minerals in the form of Sn^{4+} as same as in the case of Ge^{4+} contents in galloplumbogummite (Schlüter et al. 2014). Tetravalent components on the trivalent cation site of studied samples are compensated by a change of ratio of $(PO_3OH)^{2-}/(PO_4)^{3-}$ groups in crystal structure. An additional excess of positive charge is probably compensated by the increased amount of OH groups. The source of Sn for the formation of these minerals is probably sphalerite, in which concentrations of up to up to 3040 ppm have been measured. Other Sn-bearing minerals have not yet been identified at the deposit.

Acknowledgements. The authors would like to thank L. Váchová (National Museum, Prague) for acquiring BSE photos, also three anonymous reviewers, the editor-in-chief Vladislav Rapprich and the handling editor Roman Skála for comments and suggestions that helped to improve the manuscript. This work was financially supported by the Ministry of Culture of the Czech Republic (strategic research plan DKRVO 2024-2028/1.II.a; National Museum, 00023272).

References

Aleksandrov SM (2010) Skarn-greisen deposits of the lost river and mount ear ore field, Seward Peninsula Alaska. United States Geochem Int 48(12): 1220–1236

Åmli R, Griffin WL (1972) Three Minerals New to Norway: Wickmannite, Leadhillite and Hydrocerussite Contribution to the mineralogy of Norway, No 47. Norsk Geologisk Tidsskrift 52: 193–196

Basciano LC, Peterson RC, Roeder PL (1998) Description of schoenfliesite, $MgSn(OH)_6$, and roxbyite, $Cu_{1.72}S$, from a 1375 BC shipwreck, and Rietveld neutron-diffraction refinement of synthetic schoenfliesite, wickmanite, $MnSn(OH)_6$, and burtite, $CaSn(OH)_6$, Canad Mineral 36: 1203–1210

Bayliss P, Kolitsch U, Nickel EH, Pring A (2010) Alunite supergroup: recommended nomenclature. Mineral Mag 74: 919–927

Betterton J, Green DI, Jewson C, Spratt J, Tandy P (1998) The composition and structure of jeanbandyite and natanite. Mineral Mag 62(5): 707–712

Brandmayr M, Dallmeyer RD, Handler R, Wallbecher E (1995) Conjugate shear zones in the Southern Bohemian Massif (Austria): implications for Variscan and Alpine tectonothermal activity. Tectonophysics 248: 97–116

Čech V, Kořan J, Koutek J (1952) The ore deposits at Ratibořské Hory and Stará Vožice near Tábor. Geotechnica 13: 1–72. Praha (in Czech)

Černý P, Masau M, Ercit TS, Chapman R, Chackowsky LE (2001) Stannite and këwhile from the Peerless pegmatite, Black Hills, South Dakota, USA. J Geosci 46(1–2): 27–33

Farmer VC (1974) The Infrared Spectra of Minerals. Mineralogical Society Monograph 4. Mineral Soc London: 331–363

Faryad SW, Nahodilová R, Dolejš D (2010) Incipient eclogite facies metamorphism in the Moldanubian granulites revealed by mineral inclusions in garnet. Lithos 144: 54–69

Fiala J (1995) General characteristics of the Moldanubian zone. – In: Dallmeyer R D, Franke W, Weber K (eds) Pre-Permian Geology of Central and Eastern Europe. Springer-Verlag, Berlin Heidelberg, pp 417–418

Franke W (2000) The mid-European segment of the Variscides: tectonostratigraphic units, terrane boundaries and plate tectonic evolution. In: Franke W, Haak V, Oncken O, Tanner D (eds) Orogenic Processes: Quantification and Modelling in the Variscan Belt. Geological Society of London Special Publications 179, pp 35–61

Friedl G, Cooke RA, Finger F, McNaughton NJ, Fletcher IR (2011) Timing of Variscan HP–HT metamorphism in the Moldanubian Zone of the Bohemian Massif: U–Pb SHRIMP dating on multiply zoned zircons from a granulite from the Dunkelsteiner Wald Massif, Lower Austria. Mineral Petrol 102: 63–75

Frost RL, Sejkora J, Keeffe EC, Plášil J, Čejka J, Bahfenne S (2010) Raman spectroscopic study of the phosphate mineral churchite-(Y) $YPO_4 \cdot 2H_2O$. J Raman Spectrosc 41(2): 202–206

Frost RL, Palmer SJ, Xi Y, Čejka J, Sejkora J, Plášil J (2013) Raman spectroscopic study of the hydroxyphosphate mineral plumbogummite $PbAl_3(PO_4)_2(OH, H_2O)_6$. Spectrochim Acta A: Molecul Biomolecul Spectrosc 103: 431–434

Grey IE, Mumme WG, Bordet P, Mills SJ (2008) A new crystal-chemical variation of the alunite-type structure in monoclinic $PbZn_{0.5}Fe_3(AsO_4)_2(OH)_6$. Canad Mineral 46: 1355–1364

Grey IE, Mumme WG, Mills SJ, Birch WD, Wilson NC (2009) The crystal chemical role of zinc in alunite-type minerals: structure refinements for pure and zincian kintoreite. Amer Miner 94: 676–683

Haase P, Christensen HG, Nielsen UG, Koch CB, Galazka Z, Majzlan J (2021) Stability and solubility of members of tin perovskites in the schoenfliesite subgroup, $□_2(BSn^{4+})(OH,O)_6$ (B = Ca, Fe^{3+}, Mg, Mn^{2+}, Zn, Cu). Chem Thermodyn Therm Anal, 1–2, Article 100005

Holub V (2001) The occurrences of the Permo–Carboniferous sequences in the Blanice Graben. In: Pešek J, Holub V, Jaroš J, Malý L, Martínek K, Prouza V, Spudil J, Tásler R (eds) Geology and Deposits of Upper Paleozoic Limnic Basins of the Czech Republic. Czech Geological Survey, Prague, pp 197–207 (in Czech)

Jambor JL (1999) Nomenclature of the alunite supergroup. Canad Mineral 37: 1323–1341

Jambor JL, Dutrizac JE (1983) Beaverite–plumbojarosite solid solutions. Canad Mineral 21: 101–113

Kocourková-Víšková E, Loun J, Šráček O, Houzar S, Filip J (2014) Secondary arsenic minerals and arsenic mobility in a historical waste rock pile at Kaňk near Kutná Hora, Czech Republic. Mineral Petrol 109(1): 17–33

Kolitsch U, Pring A (2001) Crystal chemistry of the crandallite, beudantite, and alunite groups: A review and evaluation of the suitability as storage materials for toxic metals. J Mineral Petrol Sci 96: 67–78

Košler J, Kelley SP, Vrána S (2001) 40Ar/39Ar hornblende dating of a microgranodiorite dyke: implications for early Permian extension in the Moldanubian Zone of the Bohemian Massif. Int J Earth Sci (Geol Rundsch) 90: 379–385

Majzlan J, Lazic B, Armbruster T, Johnson MB, White MA, Fisher RA, Plášil J, Loun J, Škoda R, Novák M (2012) Crystal structure, thermodynamic properties, and paragenesis of bukovskýite, $Fe_2(AsO_4)(SO_4)(OH) \cdot 9H_2O$. J Mineral Petrol Sci 107(3): 133–148

Mills SJ, Grey IE, Mumme WG, Miawaki R, Matsubara S, Bordet P, Birch WD, Raudsepp M (2008) Kolitschite, $Pb[Zn_{0.5}□_{0.5}]Fe_3(AsO_4)_2(OH)_6$, a new mineral from the Kintore opencut, Broken Hill, New South Wales. Austral J Mineral 14: 63–67

Mills SJ, Kampf AR, Raudsepp M, Christy AG (2009) The crystal structure of Ga-rich plumbogummite from Tsumeb, Namibia. Mineral Mag 73: 837–845

Moura MA, Botelho NF, Carvalho de Mendonça F (2007) The indium-rich sulfides and rare arsenates of the Sn–In-mineralized Mangabeira A-type granite, central Brazil. Canad Mineral 45: 485–496

Nakamoto K (2009) Infrared and Raman spectra of inorganic and coordination compounds, Part A, Theory and applications in inorganic chemistry. 6th ed. John Wiley & Sons, Inc, Hoboken, New Jersey, pp 1–419

Nefedov EI, Griffin WL, Kristiansen R (1977) Minerals of the schoenfliesite–wickmanite series from Pitkäranta, Karelia, U.S.S.R. Canad Mineral 15: 437–445

Pačes T (1958) Příspěvek k chemismu rudních žil ze Staré Vožice u Tábora. Čas Mineral Geol 3: 43–48

Pechkovski VV, Melnikova PY, Dzyubova ED, Barannikova MV, Nikanovich M (1981) Atlas of Infrared Spectra of Phosphates. Orthophosphates. Nauka Moscow (in Russian), pp 1–248

Pouchou J, Pichoir F (1985) "PAP" (ϕρZ) procedure for improved quantitative microanalysis. In: Armstrong JT (ed) Microbeam Analysis. San Francisco Press, San Francisco, pp 104–106

Pring A, Birch WD, Dawe J. Taylor M, Deliens M, Walenta K (1995) Kintoreite, $PbFe_3(PO_4)_2(OH, H_2O)_6$, a new mineral of the jarosite-alunite family, and lusungite discredited. Mineral Mag 59: 146–148

Rattray KJ, Taylor MR, Bevan DJM, Pring A (1996) Compositional segregation and solid solution in the lead-dominant alunite-type minerals from Broken Hill, N.S.W. Mineral Mag 60: 779–785

Sato E, Nazai I, Terada Y, Tsutsumi Y, Yokoyama K, Miawaki R, Matsubara S (2008) Study of Zn-bearing beaverite $Pb(Fe_2Zn)(SO_4)_2(OH)_6$ obtained from Mikawa mine, Niigata Prefecture, Japan. J Mineral Petrol Sci 103: 141–144

Schlüter J, Malcherek T, Mihailova B (2014) Galloplumbogummite from Tsumeb, Namibia, a new member of the alunite group with tetravalent charge balance. N Jb Mineral, Abh 191: 301–309

Scott KM (1987) Solid solution in, and classification of, gossan-derived members of the alunite–jarosite family, northwest Queensland, Australia. Amer Miner 72: 178–187

Sejkora J, Čejka J, Šrein V (2001) Pb dominant members of crandallite group from Cínovec and Moldava deposits, Krušné hory Mts. (Czech Republic). J Czech Geol Soc 46(1–2): 53–68

Sejkora J, Škovíra J, Čejka J, Plášil J (2009) Cu-rich members of the beudantite–segnitite series from the Krupka ore district, the Krušné hory Mountains, Czech Republic. J Geosci 54: 355–371

Sharko ED (1971) Nature and properties of varlamoffite (oxidation products of stannite). Int Geol Rev 13(4): 603–614

Strnad L, Mihaljevič M, Šebek, O (2005) Laser ablation and solution ICP-MS determination of REE in USGS BIR-1G, BHVO-2G and BCR-2G glass reference materials. Geostand Geoanal Res 29: 303–314

Strnad L, Ettler V, Mihaljevič M, Hladil J, Chrastný V (2009) Determination of trace elements in calcite using solution and laser ablation ICP-MS: calibration to SRM NIST glass and USGS MACS carbonate and application to real landfill calcites. Geostand Geoanal Res 33: 347–355

Strnad L, Goliáš V, Mihaljevič M, Pudilová M (2012) The Variscan Kašperské Hory orogenic gold deposit, Bohemian Massif, Czech Republic. Ore Geol Rev 48: 428–441

Šrein V (1985) Mineralogical research of selected localities of the task "Evaluation of prognosis of Ag sources in the Bohemian Massif". MS Úst Geol Geotechn ČSAV. Praha (in Czech)

Velebil D, Macek I, Soumar J (2016) A contribution to knowledge of chemistry of tetrahedrites from the Czech localities: Příbram, Obecnice, Zvěstov, Mníšek pod Brdy, Ratibořské Hory, Stará Vožice, Jáchymov, Kutná Hora a Stříbrná Skalice. Bull mineral-petrolog Odd Nár Muz (Praha) 24(1): 132–143 (in Czech)

Vrtiška L, Malíková R, Dolníček Z, Sejkora J (2019a) Pyromorphite, kintoreite and cerussite from the historical Ag–Pb–Zn ore deposit Ratibořské Hory (Czech Republic). Bull Mineral Petrolog 27(2): 394–410 (in Czech)

Vrtiška L, Malíková R, Dolníček Z (2019b) Parasymplesite from the Marie Mine dump near Stará Vožice (Czech Republic). Bull Mineral Petrolog 27(2): 324–330 (in Czech)

Vrtiška L, Škácha P, Dolníček Z, Malíková R (2020) Pyrostilpnite from the Stará Vožice–Ratibořské Hory deposit (Czech Republic) Bull Mineral Petrolog 28(1): 69–73 (in Czech)

Vrtiška L, Tvrdý J, Plášil J, Sejkora J, Škoda R, Chukanov NV, Massanek A, Filip J, Dolníček Z, Veselovský F (2022) Redefinition of beraunite, $Fe^{3+}_6(PO_4)_4O(OH)_4 \cdot 6H_2O$, and discreditation of the name eleonorite: A re-investigation of type material from the Hrbek mine (Czech Republic). Eur J Mineral 34: 223–238

Zachariáš J, Hübst T (2012) Structural evolution of the Roudný gold deposit, Bohemian Massif: a combination of paleostress analysis and review of historical documents. J Geosci 57: 87–103

Zachariáš J, Paterová B, Pudilová M (2009) Mineralogy, fluid inclusion, and stable isotope constraints on the genesis of the Roudný Au–Ag deposit, Bohemian Massif. Econ Geol 104: 53–72